

Simulation of Distortions and Pattern Allowances for a Production Steel Casting

D. Galles and C. Beckermann

Department of Mechanical and Industrial Engineering, University of Iowa, Iowa City,
Iowa 52242, USA

Abstract

The dimensional inaccuracies caused by casting distortions lead to inefficiencies throughout the casting process that continue to plague industry. In this study, a finite element stress analysis code predicts dimensional changes and associated distortions for a production steel casting. Pattern allowances for several casting features are measured and later used to validate the simulations. A one-way temperature-displacement coupling uses predicted temperatures from thermal casting simulations as inputs for the stress analysis. The steel is modeled using an elasto-visco-plastic constitutive law while the bonded sand used to build the mold and cores employs the Drucker Prager Cap model. Both models are calibrated from previous experimental studies. The stress simulations quantify the predicted distortions that are created by mold expansion, core restraint, and uneven cooling. Pattern allowances are predicted with good accuracy, as the root mean square (RMS) between measured and predicted pattern allowances for the simulation is 0.29%.

1. Introduction

Casting distortions are dimensional deviations from the patternmaker's shrink (i.e., 2.1% for steel). The dimensional uncertainty that arises from distortions can lead to inefficiencies during pattern design (i.e., a time-consuming trial-and-error method) and after shakeout (i.e., post-casting operations such as welding and grinding). The source of this uncertainty can be understood from figure 1, in which measured pattern allowances from numerous castings are plotted over a range of feature lengths (taken from Voigt [2]). In the absence of distortions, all pattern allowances will be equal to the patternmaker's shrink. However, this is rarely the case in figure 1, as pattern allowances deviate both above and below patternmaker's shrink line. The considerable scatter of pattern allowances seen in figure 1 demonstrates that, due to the influence of distortions, the patternmaker's shrink cannot reliably predict pattern allowances. Therefore, another strategy is needed.

Distortions are created by 1) uneven cooling or 2) contact interactions between the casting and mold. Uneven cooling occurs in castings with different section thicknesses. These variations cause some sections to shrink faster than others, which in turn generates stresses and associated distortions. Distortions that are created from contact interactions can be attributed to several physical phenomena. For example, immediately after pouring, the bonded sand near the mold-metal interface rapidly heats and expands into the mold cavity. During this time, the molten steel offers little restraint and is displaced from the mold cavity and back into the pouring cup. This volumetric increase is not only due to thermal expansion of the sand, but as Galles and Beckermann [1] demonstrated, sand dilation as well. Sand dilation is the volumetric expansion of a granular material due to a shear force. This behavior is illustrated in figure 2; in the undisturbed state, the sand is tightly-packed and contains small air voids between the grains (figure 2(a)). After a shear force is applied, however, the irregularly-shaped sand grains translate and/or rotate and

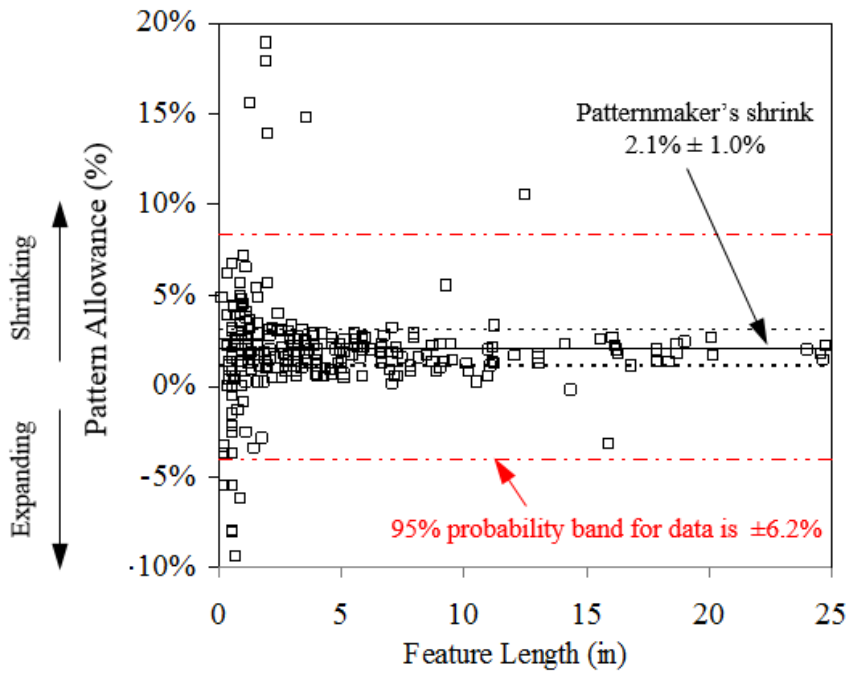


Figure 1. Measured pattern allowances plotted as a function of feature length (taken from Voigt [2]). The scatter in the data demonstrates the effect of distortions.

cause the voids to grow, resulting in expansion of the sand aggregate (figure 2(b)).

Casting simulation provides an efficient means to minimize the dimensional inaccuracies associated with distortions. In recent years, the increase in computational speeds has enabled engineers to perform finite element stress simulations using computational models that are capable of predicting distortions in castings with complex geometries and arbitrary size. The accuracy of these models is predicated on the selection of realistic constitutive laws that describe the thermomechanical behavior for both the mold and casting. Such laws must consider all important physical phenomena which lead to distortions. Furthermore, these models should be calibrated from carefully planned casting experiments. Otherwise, the reliability of the simulations cannot be trusted.

In this study, a finite element stress analysis code predicts casting distortions in a production steel casting. Pattern allowances are measured from the part at several locations and later used to validate the computational model. Simulations are performed using a one-way temperature-displacement coupling in which temperatures are calculated first using casting simulation software and then used as inputs for the finite element simulations. The steel is modeled as an elasto-visco-plastic material and the Drucker Prager Cap model is used for the sand mold and cores. Material property datasets used for the steel and sand are calibrated from previous studies [1,3]. The performance of the computational model is then evaluated by comparing the predicted pattern allowances to the measurements.

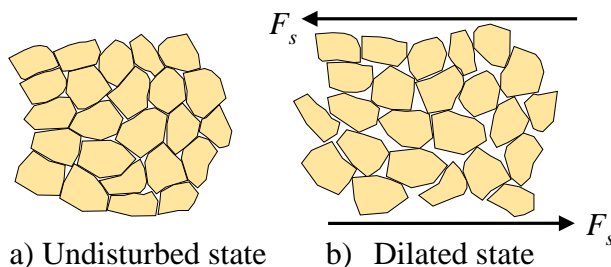


Figure 2. Sand dilation. After a shear force, F_s , is applied to the undisturbed state (a), the voids between sand grains increase, resulting in dilation (i.e., volumetric expansion of the sand aggregate), as shown by the dilated state (b).

2. Description and Dimensional Analysis of Part

The part to be analyzed in this study is a drag socket, which is used on a mining excavator to splice cables together. It was cast at the Bradken foundry in London, Ontario. The casting (shown in figure 3) has outer dimensions (in meters) of $1.91 \times 0.29 \times 0.6$ ($6.27 \times 0.95 \times 1.97$ ft) and weighs approximately 940 kg (2068 lbs). The drag socket contains several characteristics that makes it susceptible to distortions. For example, cores are needed to create the hollow interior of the main body as well as the two holes on the right side of figure 3(b). Uneven cooling is also likely to generate distortions in the varying section thicknesses of the casting as well as the gating and risers (which are not shown).

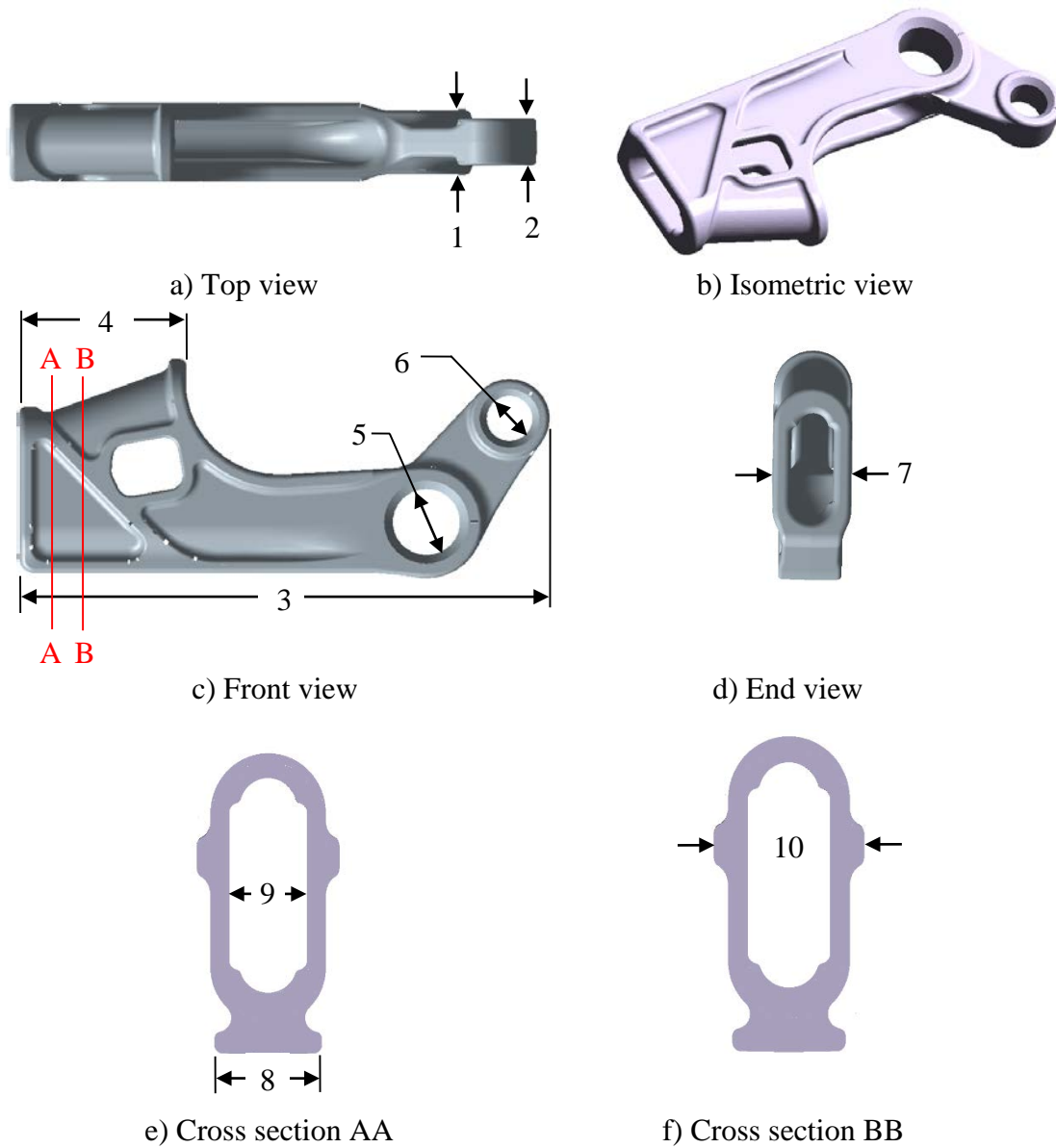


Figure 3. Casting geometry and feature lengths.

A dimensional analysis was performed after shakeout, for which several casting features were measured. Using these measurements, pattern allowances (PA) were then calculated using the relation

$$PA [\%] = \frac{feature\ length_{initial} - feature\ length_{final}}{feature\ length_{initial}} \times 100 \quad [1]$$

where $feature\ length_{initial}$ is the pattern dimension and $feature\ length_{final}$ is the casting dimension. In total, ten features were selected from the part drawing and are numbered in figure 3. A summary of the measured pattern dimensions, casting dimensions, and pattern allowances for the features are shown in table 1. Features 1, 2, 4, and 8 have pattern allowances greater than the patternmaker's shrink. This result can be explained by mold expansion. From figure 3, it can be seen that these features are measured on the outer surface of the casting. During solidification, the rapidly heating mold expands and pushes the outer walls of the casting inward to reduce feature lengths (i.e., pattern allowances are increased). These features are unconstrained and therefore, will shrink an additional 2.1% (i.e., the patternmaker's shrink) after the initial "push-in" of the outer walls, resulting in pattern allowances greater than the patternmaker's shrink. Similarly, features 3, 7, and 10 are also measured from the outer surface and can be expected to experience a reduction in length during solidification. However, these features are also influenced by core restraint. In contrast to mold expansion, distortions created from core restraint increase the feature lengths (i.e., reduce pattern allowances). Therefore, for features 3, 7, and 10, distortions created by mold expansion and core restraint distortions cancel each other out to some degree. For these situations, the pattern allowances should be viewed with caution; even if the patternmaker's shrink is measured, significant distortions may have occurred but are hidden due to the "cancelling out" explained above. Therefore, although the measured pattern allowances are close to the patternmaker's shrink for features 7 and 10 (1.95%), larger distortions may have occurred and potentially caused damage in the part. For situations in which features are measured on internal surfaces (i.e., features 5, 6, and 9), mold expansion increases the feature lengths (i.e., reduces pattern allowances). For example, mold expansion will expand the diameter of the large hole (feature 5) in figure 2(b). Because core restraint will also expand the diameter, pattern allowances for features measured on internal surfaces should always be less than the patternmaker's shrink. This is indeed the case for this study, as the maximum pattern allowance of features 5, 6, and 9 is 0.62%. Because the features are affected by different phenomena and in different ways, their pattern allowances vary over a large range, as seen in table 1 ($-0.89 < PA < 3.11$). For validation purposes, this variation is desirable for the present study.

Table 1. Measured Pattern Allowances.

Feature	Pattern Dimension (mm)	Casting Dimension (mm)	Pattern Allowance (%)
1	232.6	226	2.84
2	173.4	168	3.11
3	1899.6	1866	1.77
4	596.8	582	2.48
5	240.5	239	0.62
6	164.1	164	0.06
7	287.6	282	1.95
8	216.2	211	2.41
9	157.1	158.5	-0.89
10	287.6	282	1.95

3. Simulations

3.1 Thermal Simulations

Temperatures were predicted using the casting simulation software package MAGAMSOFT[®] [4]. The input parameters for the simulation (including temperature dependent thermophysical properties for the mold and casting, solid fraction, latent heat, and interfacial heat transfer coefficient) were determined in a previous study [3]. All components of the casting system (i.e., mold, casting, cores, risers, chills, etc.) were included in the simulation. Predicted temperature fields were output at a sufficient number of time steps to give a smooth temperature profile at every location in the model. The results were copied onto the finite element mesh used in the stress simulations.

3.2 Stress Simulations

To predict distortions, stress simulations were performed using the general purpose finite element code ABAQUS[®] [5]. The mold, gating, and risers were included in the simulations, as they their contributions to distortions could not be discounted. However, in order to protect the confidentiality of the casting design, these components will not be shown in the results. An elasto-visco-plastic constitutive law that features temperature-dependent rate and hardening effects was used to model the steel. For the mold, the pressure-dependent Drucker Prager Cap (DPC) law, which is commonly used to model the mechanical behavior of granular media, was employed. In addition, the DPC model can predict dilation, a feature that is not offered by simple elasto-plastic models. The boundary between the mold and casting was modeled using a contact interaction. Due to its complex geometry, tetrahedral elements were used to build the mesh. The model contained approximately 200,000 nodes and 1.1 million elements.

The elasto-visco-plastic model parameters were calibrated from in-situ casting experiments. The entire process and full description of the model is described elsewhere [3]. The Drucker Prager Cap model, as well as determination of its parameters, is also explained elsewhere [1].

To quantify the distortions created by each phenomenon (i.e., mold expansion, core restraint, uneven cooling), three simulations were performed. The first simulation (termed “thermal”) calculated thermal strains only. The pattern allowances predicted in this simulation are equal to the patternmaker’s shrink. The thermal simulation serves as a baseline; any predicted feature length that deviates from that in the thermal simulation is a distortion. In the second simulation (termed “casting only”), the outer mold was excluded. Here, distortions due to mold expansion and core restraint are not considered. Thus, distortions can only be created by uneven cooling in this simulation. The third simulation (termed “full”) includes the complete casting system and therefore, considers all the phenomena responsible for distortions. The predicted pattern allowances from this simulation will be compared to the measurements to determine the predictive capability of the computational model.

4. Results and Discussion

Predicted temperature contours from the thermal simulations are shown at 500 s and 5000 s in figure 4. Large temperature gradients can be seen throughout the casting at both times. For example, the body of the casting (left side of figure 4) cools much faster than the section near large hole on the right side. After 500 s, temperatures throughout the casting range from approximately 900°C (1652°F) to over 1400°C (2552°F). Even after 5000 s (~1.5 hours), temperatures vary by over 400°C (752°F). As a result of these variations, distortions can be expected from this uneven cooling.

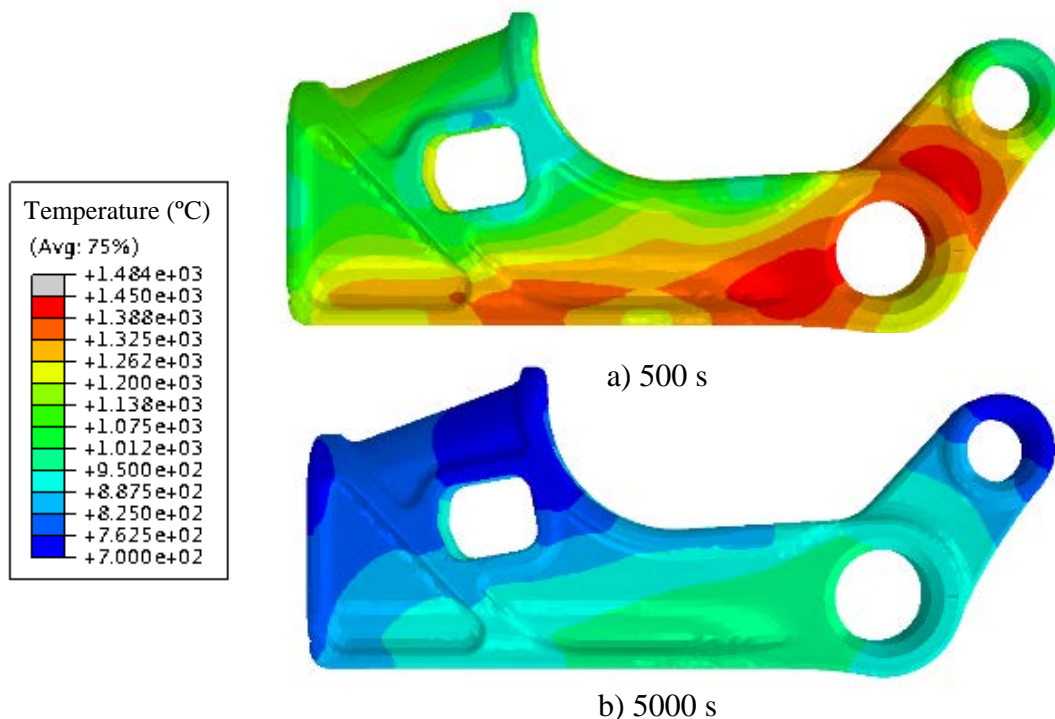


Figure 4. The predicted temperatures at 500 s (a) and 5000 s (b) reveal significant thermal gradients throughout the casting.

The deformed shape at room temperature predicted by the finite element stress simulation is shown in figure 5. The deformations are magnified by a factor of 10. The distorted shape (green) is overlaid onto the undeformed shape to illustrate where distortions occur. For example, the arm on the right side is distorted outward. Most likely, the mold impedes the thermal contractions to generate this distortion. However, uneven cooling could also have an impact. The predicted pattern allowances (shown below) will give insight to which the responsible phenomenon. Also, the holes on the right side of the casting appear to be enlarged. This is expected, as mold expansion and core restraint both can be expected to contribute to distortions of these features.



Figure 5. Deformed shape at room temperature as predicted by the finite element simulation.

The predicted temporal evolution of feature length 3 (location shown on figure 1) is plotted on complete (400,000 s) and 5000 s time scales in figure 6. The complete time scale represents the time needed to cool the casting to room temperature. For the thermal simulation (shown as the green curve), the feature length begins decreasing at approximately 500 s, which represents the approximate solidification time and is denoted by the vertical dashed line in figure 6(b). Between 500 and 400,000 s, feature length 3 decreases approximately 41.5 mm, as seen on the complete time scale in figure 6(a). This decrease occurs in the absence of distortions and represents the patternmaker's shrink. The increase in length change between 40,000 and 50,000 s is due to the solid state phase transformation from austenite to pearlite and ferrite. Differences between the casting only simulation (pink curve) and the thermal simulation can be seen beginning at 500 s. The curves gradually diverge until the end of the solid state phase transformation (at 50,000 s), after which the difference between the curves (approximately 4 mm) remains constant. Because the mold is not included in this simulation, this difference is due to uneven cooling, which distorts the arm inward. Therefore, the outward distortion observed in figure 5 must be caused by mold/core restraint. For the full simulation (blue curve), the length change during the initial 500 s (approximately -2 mm) is created by mold expansion. This expansion occurs during solidification. Once solidified, the casting has gained sufficient strength to resist any farther push-in from the mold. Beginning at 500 s, the full simulation feature length decreases at a slower rate than the thermal simulation feature length. This reduced contraction rate is due to core/mold restraint, which impedes thermal contractions and causes the feature to decrease at a slower rate than if it were unconstrained. As a result, the thermal and full simulation curves converge beginning at 500 s until they predict the same length change at 1000 s and then diverge until the beginning of the solid state

transformation (~35,000 s). Throughout this time period, considerable distortions are generated by core/mold restraint. After the solid state transformation is complete (~50,000 s), the feature lengths in the full and thermal simulation contract at the same rate, signifying that no distortions are predicted after 50,000 s. When the casting has cooled to room temperature (after approximately 400,000 s), the full simulation has reduced in length by 34 mm (see figure 6(a)). This value is very close to the measured reduction of feature length 3, which is denoted by the symbol in figure 6(a) at 400,000 s.

Similar plots for feature 5 are shown in figure 7. Very little difference can be seen between the thermal and casting only curves, which indicates that distortions created by uneven cooling are negligible for this feature. Also similar to feature 3, the solidification time occurs at approximately 500 s. Prior to 500 s, mold expansion increases feature length 5 by approximately 2.5 mm (see the full simulation curve in figure 7(b)). This result is in contrast to mold expansion for feature 3, for which mold expansion causes a decrease in the length. Recall that this is because feature length 3 is measured on the outer casting surface, whereas feature length 5 is measured on an internal surface. After feature 3 expands to a maximum value at 2000 s, its length decreases at the same rate as the thermal simulations, indicating that no distortions are predicted after 2000 s.

Through the analysis performed on feature lengths 3 and 5, several conclusions can be drawn. First, mold expansion considerably impacts feature lengths at early times. The features may either increase or decrease in length depending where they are located on the casting surface. Core/mold restraint also has a significant impact on features and always leads to increased feature lengths (i.e., decrease in pattern allowances). Finally, no distortions were predicted after the solid state phase transformation. This is not unreasonable, as the solid state phase transformation is associated with a significant increase in the casting strength.

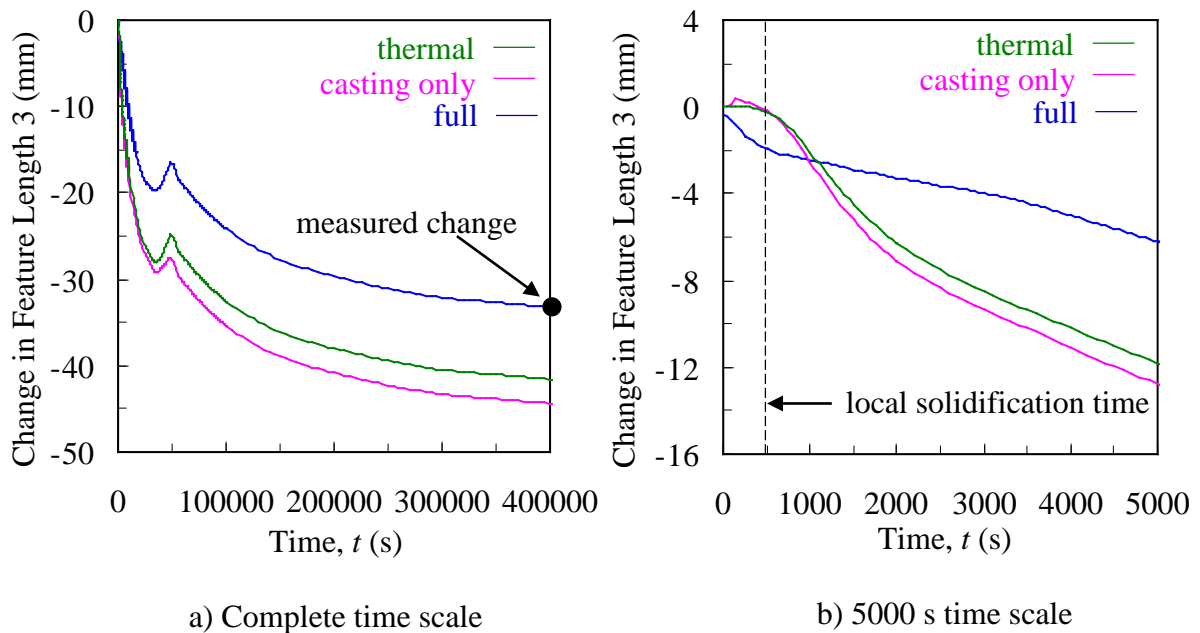


Figure 6. The predicted length changes for feature length 3 shown on complete (a) and 5000 s (b) time scales. The complete time scale represents the time needed to cool the casting to room temperature.

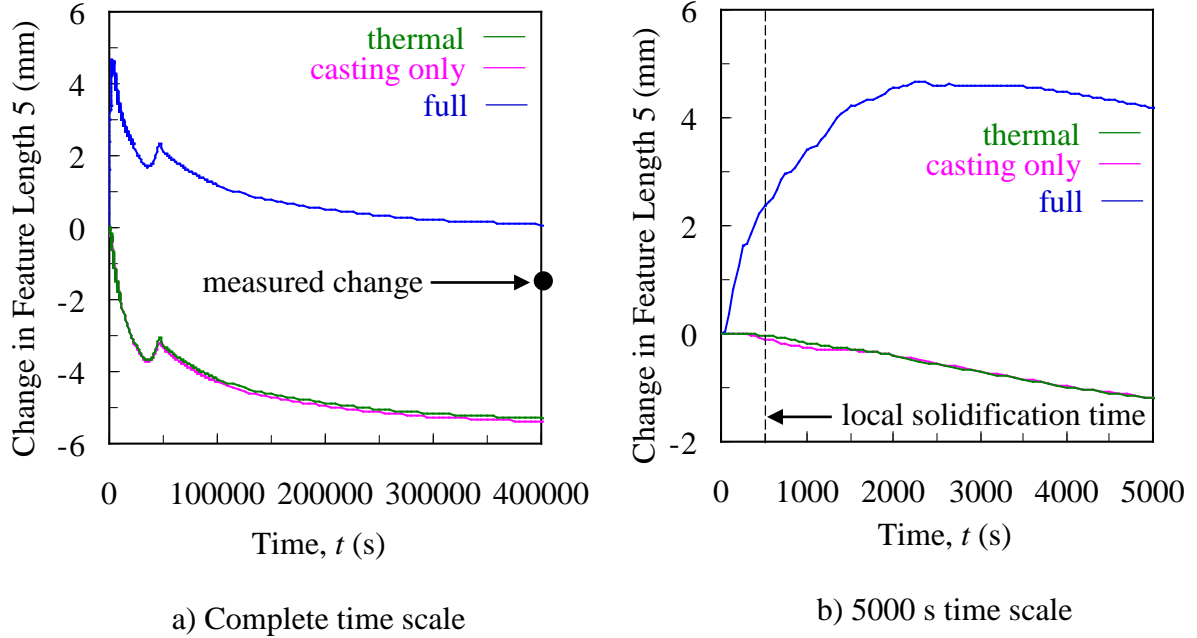


Figure 7. The predicted length changes for feature length 5 shown on complete (a) and 5000 s (b) time scales. The complete time scale represents the time needed to cool the casting to room temperature.

Comparisons between all predicted pattern allowances are compared to the measurements in figure 8. In general, the pattern allowances were predicted with good accuracy. The free shrink line is denoted by a dashed horizontal line and represents the predicted pattern allowances using the patternmaker's shrink. All of the pattern allowances (measured and predicted) are different from the free shrink. In other words, every feature chosen for this study has some amount of distortion associated with it. These distortions increase the pattern allowances for some features and decrease them for others. Even for situations where the predicted pattern allowances don't agree with the measurements, they predict the correct trends. The pattern dimensions, predicted casting dimensions, and predicted pattern allowances are summarized in table 2.

The difference between the measured and predicted pattern allowances determines the accuracy of the model. Clearly, some features were predicted more accurately than others, which can make it difficult to evaluate the overall performance of the simulation. As a solution, a suitable figure of merit that combines the predicted pattern allowances of all features into a single value should be used. However, because pattern allowances can either be positive or negative, simply taking the average of all values is not appropriate. For such cases, the root mean square (RMS) can be used. The RMS is defined as

$$PA_{RMS}[\%] = \sqrt{\frac{1}{n} \sum_{i=1}^n (PA_{measured} - PA_{predicted})^2} \quad [2]$$

Where n is the number of features, and $PA_{measured}$ and $PA_{predicted}$ are the measured and predicted pattern allowances, respectively. This number can be viewed as the average difference between measured and predicted pattern allowances. For the simulation, $PA_{RMS} = 0.29\%$. This small value demonstrates that the simulation predicts the pattern

allowances with very good accuracy. Using the RMS value, the performance of different simulations can be compared.

Contours of equivalent plastic strain and von Mises residual stress (shown in MPa) are shown in figure 9. Residual stresses are those that remain in the as cast part (i.e., before heat treatment) at room temperature. The largest residual von Mises stresses and strains occur in the body of the casting (on the left side in figure 9). Considerable plastic strains are also predicted near the two holes in the casting arm (i.e., features 5 and 6). These areas of high residual von Mises stress and strain are near locations containing cores and thus, not unexpected.

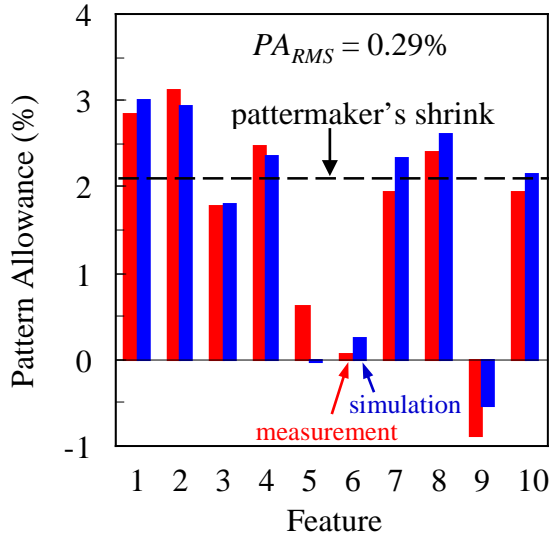


Figure 8. Comparison between measured and predicted pattern allowances. PA_{RMS} is the root mean square of the difference between predicted and measured pattern allowances.

5. Conclusions

In this study, a finite element stress analysis was performed to predict distortions for a production steel casting. Significant variations from the patternmaker's shrink (2.1%) were revealed in the measured pattern allowances, which ranged from -0.89% to 3.11%. The casting, mold, gating and risers were included in the finite element simulations and contact was used to model interactions between the mold and casting. Elasto-visco-plastic and Drucker Prager Cap constitutive laws were employed for the steel and bonded sand, respectively, and model parameters were calibrated in previous experimental studies. The computational model featured the ability to predict distortions caused by mold expansion (due to both thermal expansion and dilation), mold restraint, and uneven cooling. The simulations predicted the measured pattern allowances with good accuracy, as the root mean square (RMS) value between measured and predicted pattern allowances was calculated as 0.29%. In addition to the distortions, significant residual stresses were also predicted in the highly distorted regions of the casting. By accounting for the relevant physical phenomena that lead to distortions, the present simulations have demonstrated the ability to predict pattern allowances for a production casting. It is envisioned that such predictive capability will lead to efficient pattern design requiring fewer iterations and also minimize dimensional inaccuracies.

Table 2. Predicted pattern allowances.

Feature	Pattern Dimension (mm)	Casting Dimension (mm)	Pattern Allowance (%)
1	232.6	225.6	3.01
2	173.4	168.3	2.94
3	1899.6	1865.4	1.80
4	596.8	582.8	2.35
5	240.5	240.6	-0.02
6	164.1	163.7	0.25
7	287.6	280.9	2.32
8	216.2	210.6	2.60
9	157.1	157.9	-0.54
10	287.6	281.4	2.15

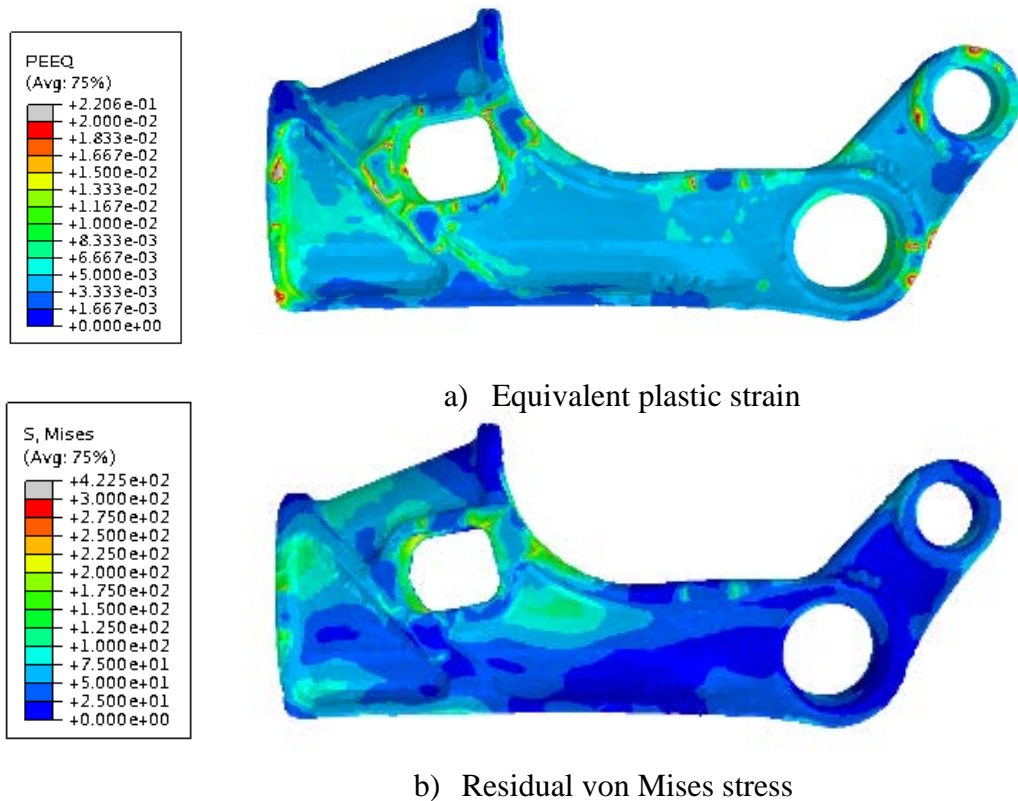


Figure 9. Predicted equivalent plastic strain and residual von Mises stress (units in MPa).

Acknowledgements

This research is sponsored by the DLA – Troop Support, Philadelphia, PA and the Defense Logistics Agency Logistics Operations, J335, Research & Development, Ft. Belvoir, VA. Also, special thanks to Vasile Ionescu and Brian Miller from Bradken-London (Casting) for their assistance and support during this study.

References

1. D. Galles and C. Beckermann, “Effect of Sand Dilation on Core Expansion during Casting of Steel”, *IOP Conf. Series: Materials Science and Engineering*, vol. 84, 2015.
2. R. Voigt, Pennsylvania State University, personal communication, 2012.
3. D. Galles, C. Monroe, and C. Beckermann, “Measurement and Prediction of Stresses during Casting of a Steel Bar”, *Proceedings of the 65th SFSA Technical and Operating Conference*, Paper No. 5.5, Steel Founders’ Society of America, Chicago, IL 2011.
4. *MAGMASoft*, MAGMA GmbH, Kackerstrasse 11, 52072 Aachen, Germany.
5. *Abaqus/Standard*, Abaqus, Inc., Providence, RI, 2006.